Control in the operational space of a redundant and under-actuated tensegrity robot

Nicolas J.S. Testard, Christine Chevallereau, Philippe Wenger

Control in the operational space of a redundant and under-actuated tensegrity robot

Nicolas J.S. Testard, Christine Chevallereau, Philippe Wenger

Nantes Université, Centrale Nantes, CNRS, LS2N, 44000 Nantes
{nicolas.testard, christine.chevallereau, philippe.wenger}@ls2n.fr

Résumé

Le contrôle d'un robot inspiré du cou d'un oiseau est proposé. Le système est composé de joints anti-parallélogrammes [1] assemblés les uns sur les autres et entraînés par des câbles de chaque côté. Le nombre d'articulations et le nombre de câbles sont choisis de manière à ce que le robot soit à la fois redondant (il y a plus d'articulations que nécessaire pour contrôler la position et l'orientation de l'effecteur du robot dans le plan) et sous-actionné (il y a plus d'articulations que de degrés de liberté pouvant être contrôlés par actionnement, l'un de ces degrés de liberté étant utilisé pour la tension des câbles). Des problèmes similaires peuvent également être rencontrés avec les robots continus [2]. Cependant, les lois de contrôle proposées dans ce domaine sont principalement basées sur la statique du robot. En revanche, la loi de commande proposée dans cet article est basée sur la dynamique du robot.

La dynamique du robot peut être exprimée par 2 équations : d'une part, les équations de Lagrange relient l'accélération des coordonnées de l'espace articulaire à la tension dans les câbles, d'autre part, le principe fondamental de la dynamique relie l'accélération des moteurs à la tension dans les câbles et aux couples appliqués dans les moteurs. La loi de commande proposée utilise ces deux équations dynamiques pour produire un mouvement dans l'espace opérationnel avec un asservissement dans l'espace opérationnel et dans l'espace moteur.

Abstract

The control of a robot inspired from a bird neck is proposed. The system is composed of anti-parallelogram joints [1] assembled on top of each other and driven by cables on each side. The number of joints and the number of cables is chosen such that the robot is both redundant (there are more joints than necessary to control the position and orientation of the robot end effector in the plane) and underactuated (there are more joints than degrees of freedom that can be controlled by actuation, with one of these degrees of freedom being used for tension in the cables). Similar problems can also be found with continuous robots [2]. However, the control laws proposed in this domain are mainly based on the statics of the robot. In contrast, the control law proposed in this paper is based on the dynamics of the robot.

The dynamics of the robot can be expressed by two equations : on the one hand, the Lagrange equations link the acceleration of the joint space coordinates to the tension in the cables, on the other hand, the fundamental principle of dynamics links the acceleration of the motors to the tension in the cables and to the torques applied in the motors. The proposed control law uses these two dynamic equations to produce a motion in the operational space with a servoing in the operational space and in the motor space.

Mots-clés : Commande, tenségrité, redondance, sous-actionnement.
Keywords : Control, tensegrity, redundant, under-actuated.

1 Introduction

The bird neck is known to be very dextrous and acts for the bird like an arm for human : it uses it to move and carry object with its beak to hold it. The neck of some birds, such as the woodpecker, can also produce high-speed movements. In this study, a planar tensegrity structure is used to model the bird neck. A tensegrity structure is composed of solid compressive elements (e.g. bars) and flexible tensile elements (e.g. cables or springs) that are assembled such that the structure is in a stable equilibrium [3]. An assembly of anti-parallelogram joints [4] actuated by two cables, derived from the Snelson X-shape mechanism [5], is used to model the bird neck. This joint, referred to as *X-joint*, models the joint between two successive vertebrae. The vertebrae are defined by the upper bars of the X-joints. The bottom bar of a given X-joint is coincident with the upper bar of the preceding X-joint. The upper bar is moved by two tendons attached at its extremities and that pulls it in two opposite directions. Springs are added in parallel of the cables such that the system has a stable equilibrium position without tension in the cables. The X-joint configuration can be modified through input forces applied in the cables.

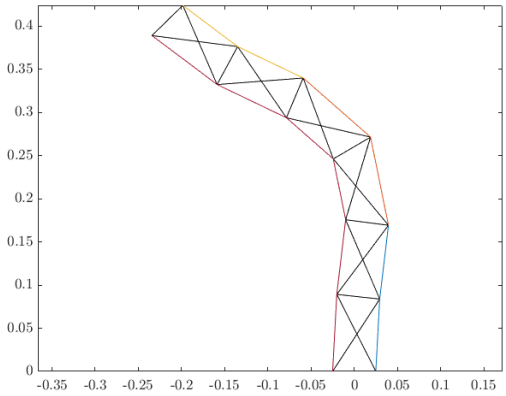

FIGURE 1 – Schematic of a tensegrity robot with 6 X-joints (black) and 4 cables (purple, blue, red, yellow).

In this study, a mechanism composed of exactly four cables actuated by four motors and at least four X-joints is used. One cable is used to actuate all the mechanisms on one side while the three others actuate one or several successive X-joints on the other side. Therefore, several X-joints will be actuated by the same cables (an example is presented in Figure 1). This cable routing is also inspired from the bird neck that has muscles connected to several vertebrae and notably a ventral muscle connected to all the vertebrae in several species. Thus, the tensegrity robot at hand is under-actuated. Since all input forces must be positive (cables cannot push), only 3 degrees of freedom can be controlled with 4 cables. Regarding the kinematic model between joint space and operational space, this model is therefore redundant since there are more than 3 joints. We propose a control law using the dynamics the robot. The dynamic equations are separated between those driving the manipulator structure and those driving the motors.

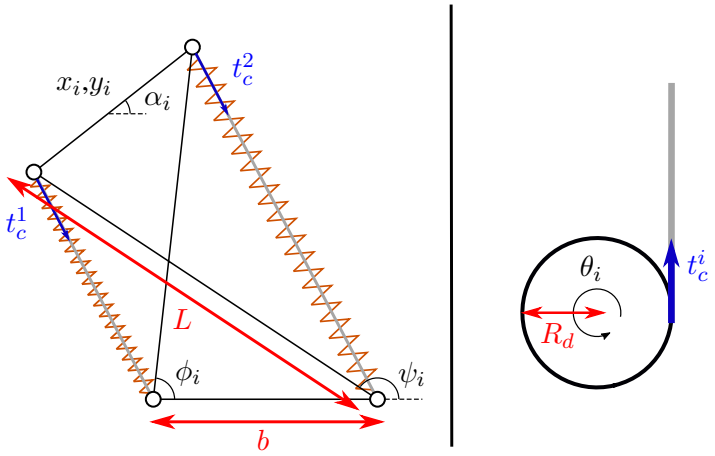

FIGURE 2 – Left : representation of the X-joint (in black) actuated by cables (in grey) in parallel with springs (in orange). Right : representation of the motor (in black) pulling the cable (in grey) through a winch

2 Kinematic modelling

All the X-joints have the same dimensions : the length of bottom and top bars is b and the length of the crossed bars is L (with the assembly condition $b \leq L$). The orientation angles ϕ_i and ψ_i of each crossed bars (Figure 2) can be calculated as functions of the top bar orientation angle α_i as shown in [6]. Therefore, the configuration of each X-joint is only defined by its angle α_i.

We define the space of the orientation angles $\alpha_i, i = 1, .., N$ of the N X-joints as the *joint space* and we define the space of the positions (x, y) and orientations γ of the end effector as the *operational space*. The relationships between the operational space $\mathbf{X} = (x, y, \gamma)$ and the joint space can be written as [7] :

$$\begin{cases} \mathbf{X} = f_X(\boldsymbol{\alpha}) \\ \dot{\mathbf{X}} = J_X \dot{\boldsymbol{\alpha}} \\ \ddot{\mathbf{X}} = J_X \ddot{\boldsymbol{\alpha}} + \dot{J}_X \dot{\boldsymbol{\alpha}} \end{cases} \tag{1}$$

Finally, we define the space of the motor positions θ_i as the *actuation space*. Each motor position θ_i is linked to the unwound cable length l_i by :

$$\theta_i = \frac{r_g}{R_d} l_i \tag{2}$$

Where R_d is the radius of the winch drum and r_g is the motor gear ratio. The length of a cable can be computed as fonction of the angle $\boldsymbol{\alpha}$ as presented in [6]. Therefore, if the cables are inelastic, the position, velocity and accelerations of the actuation space can be computed from the joint space :

$$\begin{cases} \boldsymbol{\theta} = f_\theta(\boldsymbol{\alpha}) \\ \dot{\boldsymbol{\theta}} = J_\theta \dot{\boldsymbol{\alpha}} \\ \ddot{\boldsymbol{\theta}} = J_\theta \ddot{\boldsymbol{\alpha}} + \dot{J}_\theta \dot{\boldsymbol{\alpha}} \end{cases} \tag{3}$$

3 Dynamic modelling

The Lagrange equations allows us to compute the dynamic model of our robot [8] :

$$\frac{d}{dt}\left(\frac{\partial T}{\partial \dot{\boldsymbol{\alpha}}}\right) - \frac{\partial T}{\partial \boldsymbol{\alpha}} + \frac{\partial V}{\partial \boldsymbol{\alpha}} = \Gamma \tag{4}$$

Where T is the kinetic energy, V the potential energy and Γ the generalized efforts.

After taking into account frictions, the Lagrange equations can be rewritten as follows (see [9], [10] for more details) :

$$\mathbf{M}_{\alpha}^{s}\ddot{\boldsymbol{\alpha}} + \mathbf{c}_s(\dot{\boldsymbol{\alpha}}, \boldsymbol{\alpha}) + \mathbf{g}(\boldsymbol{\alpha}) = \mathbf{Z}\left(\mathbf{t}_c - \mathbf{f}_{rc}\right) - \boldsymbol{\Gamma}_{r\alpha} \tag{5}$$

Where $\mathbf{M}_{\alpha}^{s}$ is the inertia matrix of the structure, $\mathbf{c}_s(\dot{\boldsymbol{\alpha}}, \boldsymbol{\alpha})$ are the Coriolis and centripetal effects, $\mathbf{g}(\boldsymbol{\alpha})$ corresponds to the effect of the gravity and the effect of the springs in parallel of the cables, $\mathbf{Z}$ is a $N \times 4$ matrix linked to J_θ by $\mathbf{Z} = -\frac{r_g}{R_d} J_\theta^\top$, $\mathbf{t}_c$ are the tension in the cables, $\mathbf{f}_{rc}$ are the friction in the cables and $\boldsymbol{\Gamma}_{r\alpha}$ are the resistive torques produced by friction in the X-joints.

The dynamics of one motor (Figure 2, right) can be derived using the fundamental principle of the dynamics :

$$I_\theta \ddot{\theta}_i = \Gamma_m^i - \Gamma_{r\theta}^i + \frac{R_d}{r_g} t_c^i \tag{6}$$

Where I_θ is the equivalent inertia resulting from the inertia of the motor, the inertia of the gear and the inertia of the drum. Γ_m^i is the motor torque, $\Gamma_{r\theta}^i$ is the friction in the motor and t_c^i is the tension of the cable attached to the motor.

The dynamic of all the motors, which are identical, can be collected into one equation :

$$M_\theta^m \ddot{\boldsymbol{\theta}} = \boldsymbol{\Gamma}_m - \boldsymbol{\Gamma}_{r\theta} + \frac{R_d}{r_g} \mathbf{t}_c \tag{7}$$

Where $M_\theta^m = diag(I_\theta), \boldsymbol{\Gamma}_m = [\Gamma_m^1, \Gamma_m^2, \Gamma_m^3, \Gamma_m^4]^\top, \boldsymbol{\Gamma}_{r\theta} = [\Gamma_{r\theta}^1, \Gamma_{r\theta}^2, \Gamma_{r\theta}^3, \Gamma_{r\theta}^4]^\top$ and $\mathbf{t}_c = [t_c^1, t_c^2, t_c^3, t_c^4]^\top$.

4 Proposed control law

4.1 Computed torque control in the operational space

Since the robot at hand is kinematically redundant, an infinity of configurations in the joint space exist to follow a prescribed trajectory (X_d,$\dot{X}_d$ and $\ddot{X}_d$) in the operational space defined in position, orientation and acceleration. However, these configurations are not all feasible because the robot is under-actuated The idea is then to manipulate Eq. (5) in order to express the dynamic of the acceleration in the operational space as a function of cable tensions and, finally to apply a computed torque control. First, one can multiply the equation by the inverse of the inertia matrix and express $\ddot{\boldsymbol{\alpha}}$ as :

$$\ddot{\boldsymbol{\alpha}} = (\mathbf{M}_{\alpha}^{s})^{-1}\left(\mathbf{Z}\left(\mathbf{t}_c - \mathbf{f}_{rc}\right) - \mathbf{c}_s(\dot{\boldsymbol{\alpha}}, \boldsymbol{\alpha}) - \mathbf{g}(\boldsymbol{\alpha}) - \boldsymbol{\Gamma}_{r\alpha}\right) \tag{8}$$

From Eq. (1), we obtain :

$$\ddot{\mathbf{X}} = J_X(\mathbf{M}_{\alpha}^{s})^{-1}\left(\mathbf{Z}\left(\mathbf{t}_c - \mathbf{f}_{rc}\right) - \mathbf{c}_s(\dot{\boldsymbol{\alpha}}, \boldsymbol{\alpha}) - \mathbf{g}(\boldsymbol{\alpha}) - \boldsymbol{\Gamma}_{r\alpha}\right) + \dot{J}_X\dot{\alpha} \tag{9}$$

Let $\mathbf{Z}_X = J_X(\mathbf{M}_\alpha^s)^{-1}\mathbf{Z}$, $\mathbf{c}_X(\dot{\boldsymbol{\alpha}}, \boldsymbol{\alpha}) = J_X(\mathbf{M}_\alpha^s)^{-1}\mathbf{c}_s(\dot{\boldsymbol{\alpha}}, \boldsymbol{\alpha})$, $\mathbf{g}_X(\boldsymbol{\alpha}) = J_X(\mathbf{M}_\alpha^s)^{-1}\mathbf{g}(\boldsymbol{\alpha})$ and $\boldsymbol{\Gamma}_{r\alpha X} = J_X(\mathbf{M}_\alpha^s)^{-1}\boldsymbol{\Gamma}_{r\alpha}$. The preceding equation can be written as :

$$\ddot{\mathbf{X}} - \dot{J}_X\dot{\boldsymbol{\alpha}} + \mathbf{c}_X(\dot{\boldsymbol{\alpha}}, \boldsymbol{\alpha}) + \mathbf{g}_X(\boldsymbol{\alpha}) = \mathbf{Z}_X\left(\mathbf{t}_c - \mathbf{f}_{rc}\right) - \boldsymbol{\Gamma}_{r\alpha X} \tag{10}$$

We then obtain an equation linking the acceleration in the operational space to the cable tension. Our objective is that the end-effector in closed loop evolves as : $\ddot{\mathbf{X}} = \mathbf{w}_X$ where $\mathbf{w}_X$ corresponds to a PID (Proportional Integrate Derivative) servoing expressed in the operational space :

$$\mathbf{w}_X = \ddot{\mathbf{X}}_d + K_p^X(\mathbf{X}_d - \mathbf{X}) + K_d^X(\dot{\mathbf{X}}_d - \dot{\mathbf{X}}) + K_i^X\int(\mathbf{X}_d - \mathbf{X})dt \tag{11}$$

Where K_p^X, K_d^X and K_i^X are constants chosen to insure a stable behaviour.

Let us define $\boldsymbol{\Gamma}_d$ as :

$$\boldsymbol{\Gamma}_d = \mathbf{w}_X - \dot{J}_X\dot{\boldsymbol{\alpha}} + \mathbf{c}_X(\dot{\boldsymbol{\alpha}}, \boldsymbol{\alpha}) + \mathbf{g}_X(\boldsymbol{\alpha}) + \boldsymbol{\Gamma}_{r\alpha X} \tag{12}$$

Since matrix $\mathbf{Z}_X$ is of dimension 3×4, positive cable tensions can be defined with one degree of freedom and Eq. (10) yields :

$$\left(\mathbf{t}_c - \mathbf{f}_{rc}\right) = \mathbf{Z}_X^+\boldsymbol{\Gamma}_d + \mathbf{N}_{\mathbf{Z}_X}\lambda_F \tag{13}$$

where $\mathbf{N}_{\mathbf{Z}_X}$, a vector of dimension 4, is the null space of $\mathbf{Z}_X$ and λ_F is a scalar defined such that all the tensions are greater than a predefined minimal value.

4.2 Computed torque control in the actuation space

Equation (13) allows computing the desired tension in the cables. However, the acceleration in the actuation space is also required to compute the motor torques in Eq. (7). Nonetheless, there is no direct equation linking the acceleration in the actuation space to the one in the operational space. From Eq. (1), the set of joint configurations that allows tracking the desired trajectory in the operational space can be expressed as :

$$\begin{cases} \Delta\boldsymbol{\alpha} = J_X^+\Delta\mathbf{X} + \mathbf{N}_{J_X}\boldsymbol{\lambda}_\alpha \\ \dot{\boldsymbol{\alpha}} = J_X^+\dot{\mathbf{X}} + \mathbf{N}_{J_X}\boldsymbol{\lambda}_{\dot{\alpha}} \\ \ddot{\boldsymbol{\alpha}} = J_X^+(\ddot{\mathbf{X}} - \dot{J}_X\dot{\boldsymbol{\alpha}}) + \mathbf{N}_{J_X}\boldsymbol{\lambda}_{\ddot{\alpha}} \end{cases} \tag{14}$$

where $\mathbf{N}_{J_X}$ is the null space of J_X (dimension $(N-3)\times N$) and $\boldsymbol{\lambda}_\alpha$, $\boldsymbol{\lambda}_{\dot{\alpha}}$ $\boldsymbol{\lambda}_{\ddot{\alpha}}$ are 3 vectors of dimension $N-3$. These vectors are difficult to determine as they also depend on the forces that need to be computed. Therefore, we hypothesize that the real resulting joint configuration is close to the case where these vectors are null. With this hypothesis, we insure null joint velocities and accelerations for a static configuration. Therefore, the result corresponds to the minimization of the norm of $\Delta\boldsymbol{\alpha}$, $\dot{\boldsymbol{\alpha}}$ and $\ddot{\boldsymbol{\alpha}}$. Thus, the desired positions, velocities and acceleration in the joint space are :

$$\begin{cases} \boldsymbol{\alpha}_d = \boldsymbol{\alpha} + J_X^+(\mathbf{X}_d - \mathbf{X}) \\ \dot{\boldsymbol{\alpha}}_d = J_X^+\dot{\mathbf{X}}_d \\ \ddot{\boldsymbol{\alpha}}_d = J_X^+(\ddot{\mathbf{X}}_d - \dot{J}_X\dot{\boldsymbol{\alpha}}) \end{cases} \tag{15}$$

Their corresponding values in the actuation space are :

$$\begin{cases} \boldsymbol{\theta}_d = f_\theta(\boldsymbol{\alpha}_d) \\ \dot{\boldsymbol{\theta}}_d = J_\theta \dot{\boldsymbol{\alpha}}_d \\ \ddot{\boldsymbol{\theta}}_d = J_\theta \ddot{\boldsymbol{\alpha}}_d + \dot{J}_\theta \dot{\boldsymbol{\alpha}} \end{cases} \tag{16}$$

In Eq. (7), a PID servoing on the acceleration in the actuation space can thus be carried out as follows :

$$\mathbf{w}_\theta = \ddot{\boldsymbol{\theta}}_d + K_p^\theta \left(\boldsymbol{\theta}_d - \boldsymbol{\theta}\right) + K_d^\theta \left(\dot{\boldsymbol{\theta}}_d - \dot{\boldsymbol{\theta}}\right) + K_i^\theta \int \left(\boldsymbol{\theta}_d - \boldsymbol{\theta}\right) dt \tag{17}$$

$$\boldsymbol{\Gamma}_m = \mathbf{M}_\theta^m \mathbf{w}_\theta + \boldsymbol{\Gamma}_{r\theta} - \frac{R_d}{r_g} \mathbf{t}_c \tag{18}$$

Where K_p^θ, K_d^θ and K_i^θ are constants.

This servoing is based on an hypothesis on the evolution of the joints to satisfy a desired trajectory in the operational space. The first computed torque control applied directly in the operational space therefore compensates the error on the estimated evolution of the joint. If the error in the operational space is low, the error in the joint space will be low as well and the computed torque control in the actuation space will not diverge. Especially, when the robot is not moving, the desired configuration in the joint space is the correct one.

The scheme of the control law is shown in Figure 3.

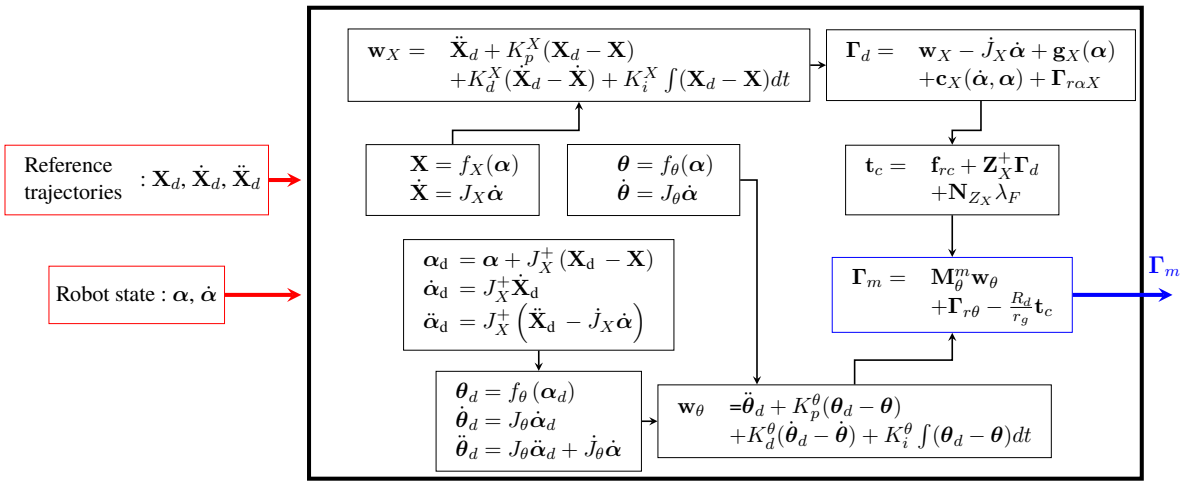

FIGURE 3 – Control law in the operational space

5 Simulation

5.1 Parameters of the simulation

For the simulation, the friction in the motor $\Gamma_{r\theta}$ and in the cables f_{rc} are neglected and the friction in the joints corresponds to viscous friction of the form $\Gamma_{r\alpha} = 2f_v(\frac{\partial\phi}{\partial\alpha}^2 + \frac{\partial\psi}{\partial\alpha}^2)\dot{\alpha}$ where f_v is a constant friction, identical for all joints. The elasticity in the cable is associated to a spring $t_c = k_c x_c$, where k_c is the cable stiffness. The bars of the X-joints are considered symmetric and all the X-joints have the same dimensions. The values of the different parameters are given in Table 1.

b	5 cm
L	10 cm
m short bar	0.014 kg
m long bar	0.02 kg
I short bar	7e-6 kg.m²
I long bar	3e-5 kg.m²
R_d	2 cm
r_g	1
I_θ	4e-6 kg.m²
k_c	1e-5 N/m
f_v	0.1 N.m/(rad/s)

TABLE 1 – Robot parameters used for the simulation

The springs that are in parallel of the cables have a free length of 4.6 cm. Their constant varies from 100 N/m to 2000 N/m, depending on the number of X-joints used. Moreover, spring constants are higher in X-joints located near the robot base.

The PID constants have been set such that :

$$\begin{cases} K_p^X = 3\omega_X^2, & K_d^X = 3\omega_X, & K_i^X = \omega_X^3 \\ K_p^\theta = 3\omega_\theta^2, & K_d^\theta = 3\omega_\theta, & K_i^\theta = \omega_\theta^3 \end{cases} \tag{19}$$

where $\omega_X = 2$ and $\omega_\theta = 20$.

The simulation is done using a time-stepping implicit scheme (backward Euler) [11] that integrates the dynamic equations.

5.2 Results

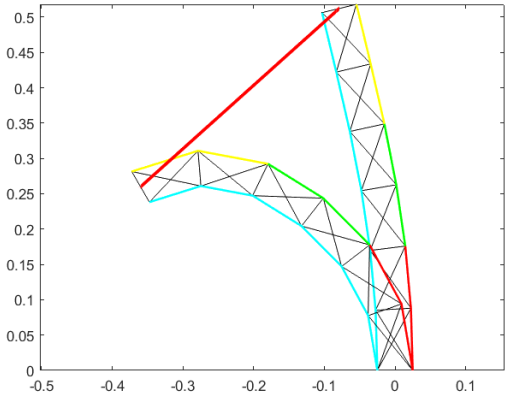

FIGURE 4 – Trajectory of the movement

Our control law has been tested for a number of joints N varying from 4 to 10 stacked X-joints and proved satisfying in every case. Results for 6 joints are presented in this section as an example. θ_1 pull a cable linked on the left side of all the joints, θ_2, respectively θ_3, respectively θ_4 pull a cable linked on the right side of the joints number 1 and 2, respectively 3 and 4, respectively 5 and 6. The springs on each side of each X-joint are identical and the value of their constant are, from base to top :800 N/m, 800 N/m,

600 N/m, 600 N/m, 400 N/m, 400 N/m. The desired trajectory is shown in Figure 4 and the minimal cable tension is set to 10 N. Figures 5, 6 and 7 show the evolution of the robot during this trajectory. In Figure 5, it can be seen that the trajectory is well followed with a mean error around 0.01 mm on the position and less than 0.001° on the orientation. These errors are linked to the estimation of the desired position, velocity and acceleration in the joint space (Eq. 14). Figure 7 shows cable tensions during the trajectory. It can be observed that it almost fully respects the limit of 10 N as minimal tension. There is an error of 0.1 N in the minimal tension. This error is linked to the addition of the computed torque control in the actuation space (Eq. 18).

Figures 8, 9 and 10 show the time histories of the robot for a desired steady state after a perturbation of -0.05 rad on all the joints from the last position of the previous trajectory. It can be observed that the control law makes the robot converge to the desired position in less than 1 s with an overshoot of the desired position in the operational space and oscillations. In the joint space, the oscillations of the angles α_4, α_5 and α_6 are very different from the oscillations of the positions in the operational space, showing the difficulty to predict the dynamic equilibrium leading to the desired evolution in the operational space. In Figure 10, it can be observed that the minimal tension is below the desired minimal one with an error of 5 N. This result is due to the jump of the angles after the perturbation to reach a stable dynamic position and to the computed torque control in the actuation space that imposes a great correction. Figure 9 also shows that the robot reaches the same joint configuration as before the perturbation to obtain the same position and orientation of the end-effector for this small perturbation. Similarly, Figure 10 shows that the forces are also the same before and after the perturbation.

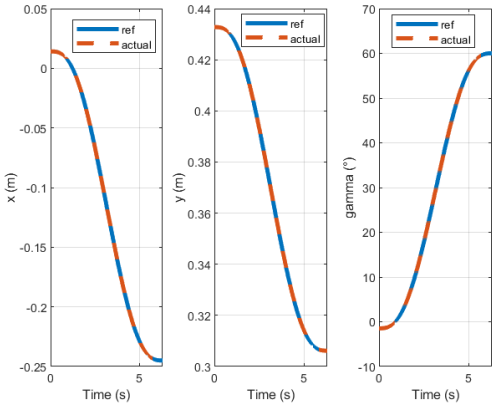

FIGURE 5 – Tracking of the trajectory

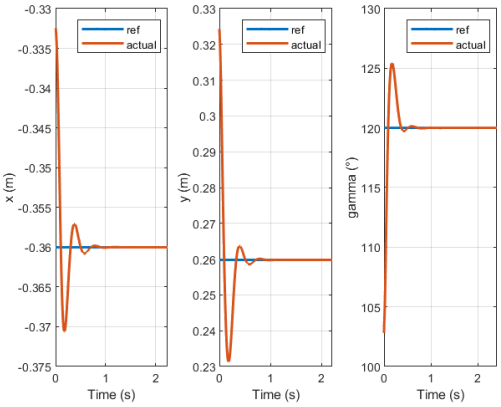

FIGURE 8 – Tracking after a perturbation

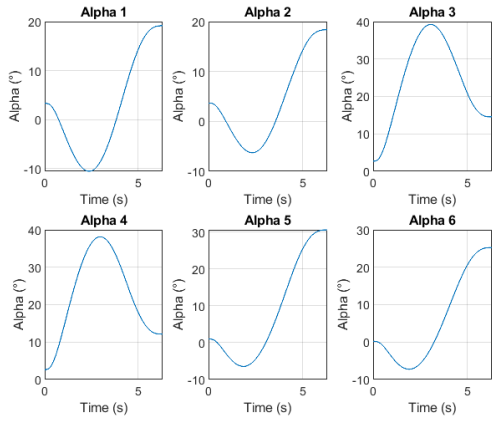

FIGURE 6 – Evolution of the joints during the trajectory

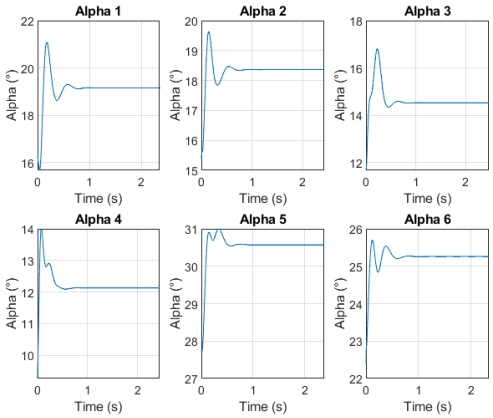

FIGURE 9 – Evolution of the joints after a perturbation

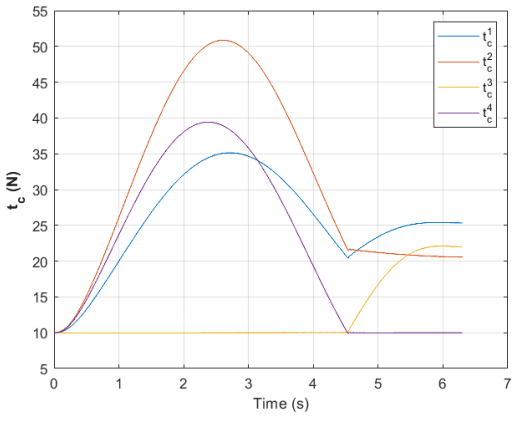

FIGURE 7 – Tension in the cables during the trajectory

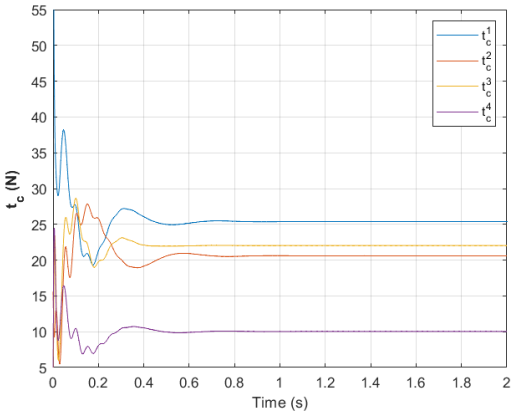

FIGURE 10 – Tension in the cables after a perturbation

6 Conclusion and future work

This article has presented a control law for the servoing in the operational space of a tensegrity robot. The important, original point is that the robot is both kinematically redundant and under-actuated, which makes it difficult to design a satisfactory control law. The control law was design upon separating the dynamics of the structure from the dynamics of the motors that are linked together by cable tensions. Two computed torque control laws have been applied, each linked to one dynamic equation. An hypothesis on the evolution of the joint space has been made to apply the PID in the actuation space. It has been observed in simulation that this control law allows the robot to follow a desired trajectory in the operational space.

A prototype with 6 modules is currently built. The control law will be tested on this prototype and friction will be identified.

Références

[1] V. Muralidharan and P. Wenger, "Optimal design and comparative study of two antagonistically actuated tensegrity joints," *Mechanism and Machine Theory*, vol. 159, p. 104249, 2021.

[2] G. Robinson and J. Davies, "Continuum robots - a state of the art," in *Proceedings 1999 IEEE International Conference on Robotics and Automation (Cat. No.99CH36288C)*, vol. 4, pp. 2849–2854 vol.4, 1999.

[3] R. Skelton and M. de Oliveira, *Tensegrity Systems*. Springer US, 2009.

[4] V. Muralidharan, P. Wenger, and M. Furet, "Static analysis and design strategy of two antagonistically actuated joints," in *New Trends in Mechanism and Machine Science* (D. Pisla, B. Corves, and C. Vaida, eds.), (Cham), pp. 459–469, Springer International Publishing, 2020.

[5] K. D. Snelson, "Continuous tension, discontinuous compression structures," *US Patent*, February 1965.

[6] A. Van Riesen, M. Furet, C. Chevallereau, and P. Wenger, "Dynamic analysis and control of an antagonistically actuated tensegrity mechanism," in *22nd CISM IFToMM Symposium on Robot Design, Dynamics and Control (ROMANSY'2018)*, vol. 584 of *ROMANSY 22 – Robot Design, Dynamics and Control Proceedings of the 22nd CISM IFToMM Symposium, June 25-28, 2018, Rennes, France*, (Rennes, France), pp. 481–490, Springer, June 2018.

[7] M. Furet and P. Wenger, "Kinetostatic analysis and actuation strategy of a planar tensegrity 2-x manipulator," *Journal of Mechanisms and Robotics*, vol. 11, no. 6, 2019.

[8] R. A. Petre, S. E. Nichifor, A. Craifaleanu, and I. Stroe, "Using lagrange equations to study the relative motion of a mechanism," *International Journal of Aerospace and Mechanical Engineering*, vol. 14, no. 10, pp. 481 – 485, 2020.

[9] B. Fasquelle, M. Furet, P. Khanna, D. Chablat, C. Chevallereau, and P. Wenger, "A bio-inspired 3-dof light-weight manipulator with tensegrity x-joints," in *2020 IEEE International Conference on Robotics and Automation (ICRA)*, pp. 5054–5060, IEEE, 2020.

[10] B. Fasquelle, P. Khanna, C. Chevallereau, D. Chablat, D. Creusot, S. Jolivet, P. Lemoine, and P. Wenger, "Identification and control of a 3-x cable-driven manipulator inspired from the bird neck," *Journal of Mechanisms and Robotics*, pp. 1–25, 2021.

[11] E. Coevoet, T. Morales-Bieze, F. Largilliere, Z. Zhang, M. Thieffry, M. Sanz-Lopez, B. Carrez, D. Marchal, O. Goury, J. Dequidt, and C. Duriez, "Software toolkit for modeling, simulation, and control of soft robots," *Advanced Robotics*, 2017.